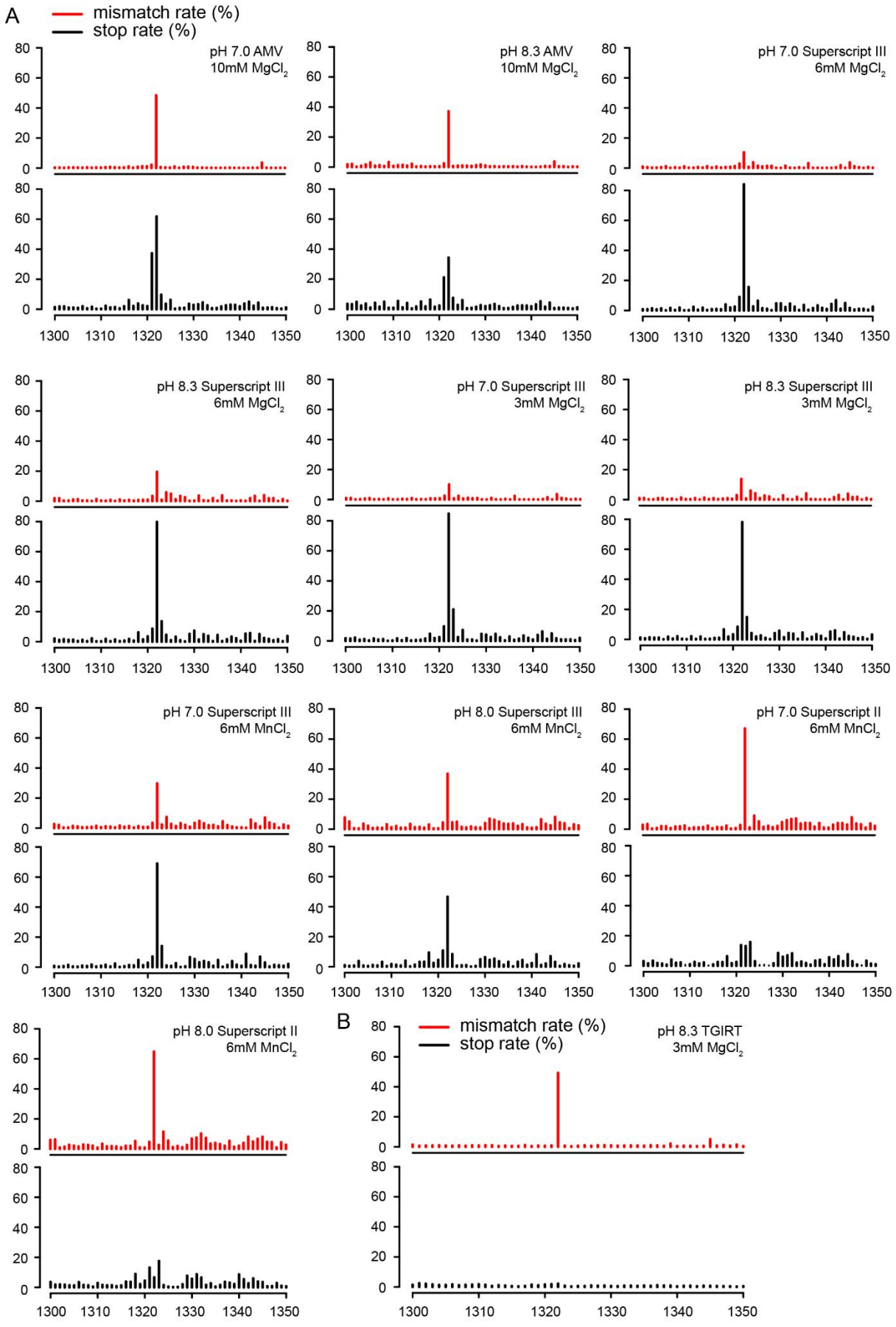
A
mismatch rate (%)
stop rate (%)
pH 7.0 AMV
10mM MgCl2
pH 8.3 AMV
10mM MgCl2
pH 7.0 Superscript III
6mM MgCl2
pH 8.3 Superscript III
6mM MgCl2
pH 7.0 Superscript III
3mM MgCl2
pH 8.3 Superscript III
3mM MgCl2
pH 7.0 Superscript III
6mM MnCl2
pH 8.0 Superscript III
6mM MnCl2
pH 7.0 Superscript II
6mM MnCl2
pH 8.0 Superscript II
6mM MnCl2
B
mismatch rate (%)
stop rate (%)
pH 8.3 TGIRT
3mM MgCl2
0
20
40
60
80
1300
1310
1320
1330
1340
1350

Figure S1. Performance of different RTases on capturing m^1A-induced mutation/truncation signature under different conditions, Related to Figure 1.

(**A**) AMV, Superscript II and Superscript III were tested under different reverse transcription (RT) conditions for their capabilities to capture the misincorporation and truncation signatures caused by m^1A. Red lines represent the mismatch rate, while black lines represent the stop rate.

(**B**) TGIRT demonstrated high signal-to-noise ratio in detecting m^1A site, with relatively high read-through efficiency and high mutation frequency.

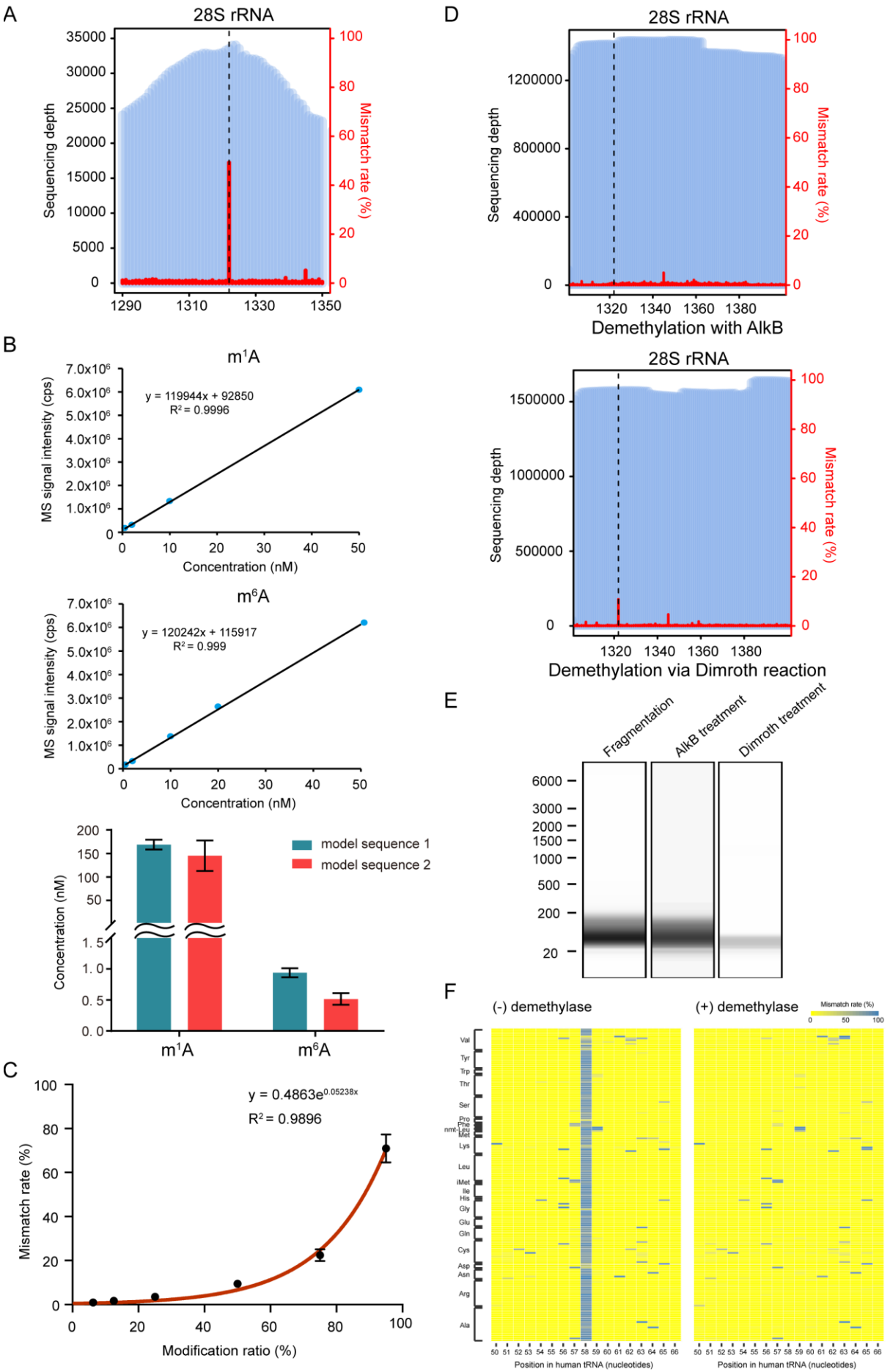
A
28S rRNA
Sequencing depth
Mismatch rate (%)
B
m¹A
y = 119944x + 92850
R² = 0.9996
MS signal intensity (cps)
Concentration (nM)
m⁶A
y = 120242x + 115917
R² = 0.999
model sequence 1
model sequence 2
Concentration (nM)
C
y = 0.4863e^0.05238x
R² = 0.9896
Mismatch rate (%)
Modification ratio (%)
D
28S rRNA
Demethylation with AlkB
Demethylation via Dimroth reaction
E
Fragmentation
AlkB treatment
Dimroth treatment
F
(-) demethylase
(+) demethylase
Mismatch rate (%)
Position in human tRNA (nucleotides)

Figure S2. Performance of m^1A-MAP on chemically synthesized model RNA sequences, as well as known sites in human rRNA and tRNA, Related to Figure 1.

(**A**) The sequencing depth of regions surrounding m^1A1322 in 28S rRNA and the corresponding mismatch rate are plotted. A mismatch rate of approximately 40-50% was observed for m^1A1322.

(**B**) The m^1A modification levels of model sequence 1 and model sequence 2 were measured by quantitative mass spectrometry (LC-MS/MS). The amount of m^6A contamination (introduced during the oligo deprotection and purification process) in the m^1A oligoes was deduced by fitting the signal intensities into the stand curve. The m^1A and m^6A standard calibration curves were obtained using five standard samples with different concentrations of pure m^1A or m^6A, respectively. The results showed that the m^1A modification level for model sequence 1 and 2 is ~97% and ~98%, respectively. Data are represented as mean ± SD; n = 4.

(**C**) Sequencing experiments to pre-mixed model RNA sequences of different m^1A modification levels. The observed mismatch rate dropped non-linearly with the decrease of actual modification level. Data are represented as mean ± SD; n = 2.

(**D**) *In vitro* demethylation reaction by the demethylase AlkB demonstrated a higher efficiency than the Dimroth reaction.

(**E**) “Fragmentation” represents the RNA sample fragmented using the regular fragmentation condition; “AlkB treatment” represents further AlkB treatment to the fragmented RNA; “Dimroth treatment” represents Dimroth reaction directly to un-fragmented RNA. Compared to AlkB treatment, Dimroth reaction can cause excessive RNA degradation even without the regular fragmentation process.

(**F**) m^1A-MAP detects m^1A58 for the cytosolic tRNAs. The mismatch rates of (-) and (+) demethylase sample are shown, respectively.

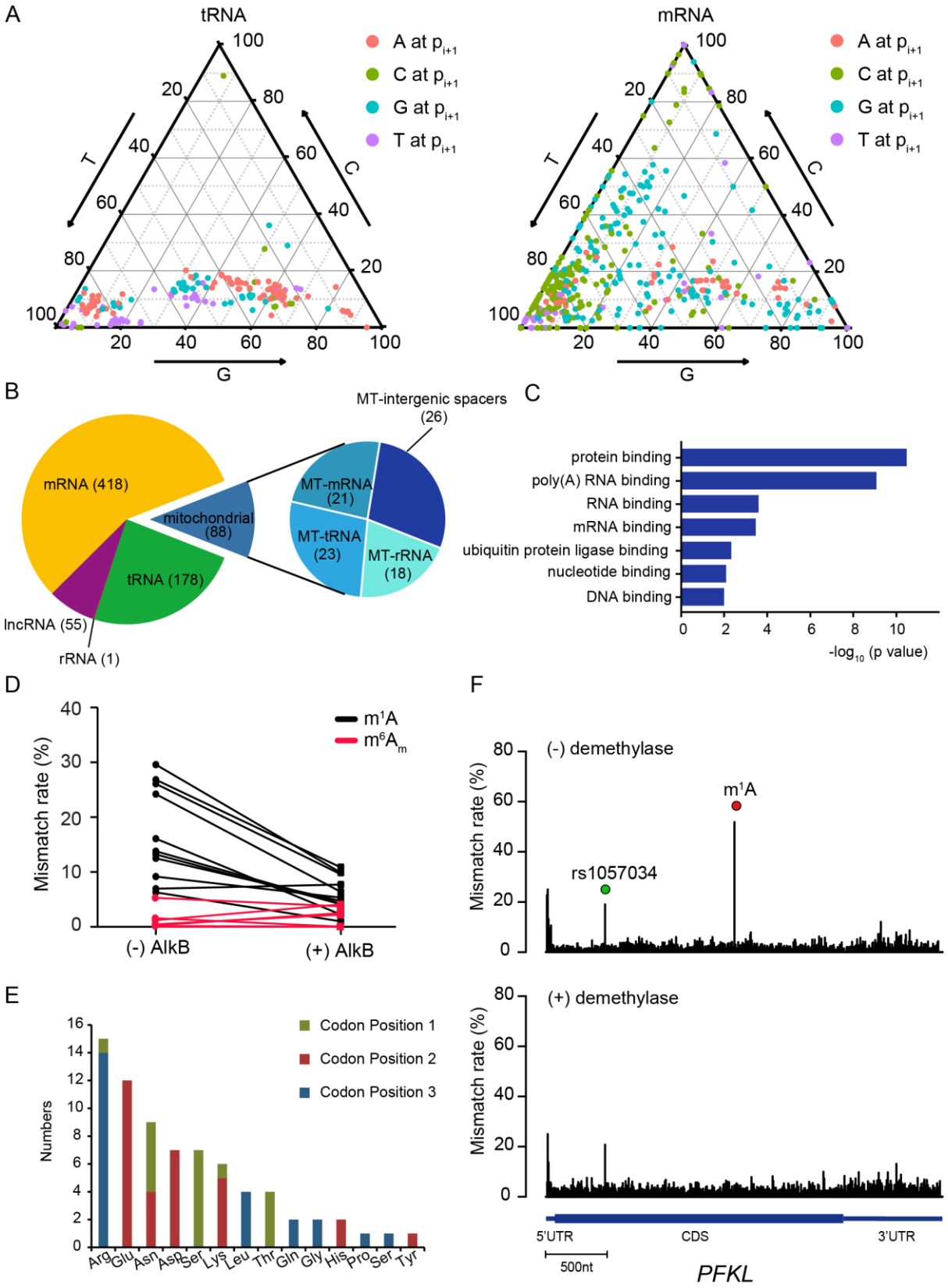

Figure S3. Single-nucleotide resolution m^{1}A methylome in the human transcriptome,

Related to Figure 2.

(**A**) Sequence-dependent mutation profiles of m^1A sites with regard to the immediate 3' nucleotide. Profiles of m^1A sites in both tRNA and mRNA are shown.

(**B**) The pie chart shows the number of m^1A sites identified in different RNA species in the human transcriptome.

(**C**) Gene Ontology analysis was performed for the nuclear-encoded mRNA containing m^1A sites. The GO terms enriched in Molecular Function (MF) are shown (p-value provided by DAVID). m^1A-containing genes tend to be enriched within the functions of protein binding and poly-A RNA binding.

(**D**) m^1A sites at the cap+1 position were validated using an antibody-independent, locus-specific assay. As a comparison, several cap+1 m^6A_m sites reported in the *Nature* Paper (Mauer et al., 2017) were also employed. The mutation rates for cap+1 m^1A sites in the "(-) AlkB" sample are relatively high, and the mutation rates of 10/11 sites drop greatly after AlkB treatment. As a comparison, the mutation rates of m^6A_m in the "(-) AlkB" sample are low, and no significant changes could be observed after AlkB treatment.

(**E**) The counts of m^1A sites in different codon positions and codon types are shown.

(**F**) A representative view of a typical m^1A site in the CDS of *PFKL*. The identified m^1A site is indicated by a red dot, while a known SNP is indicated by a green dot.

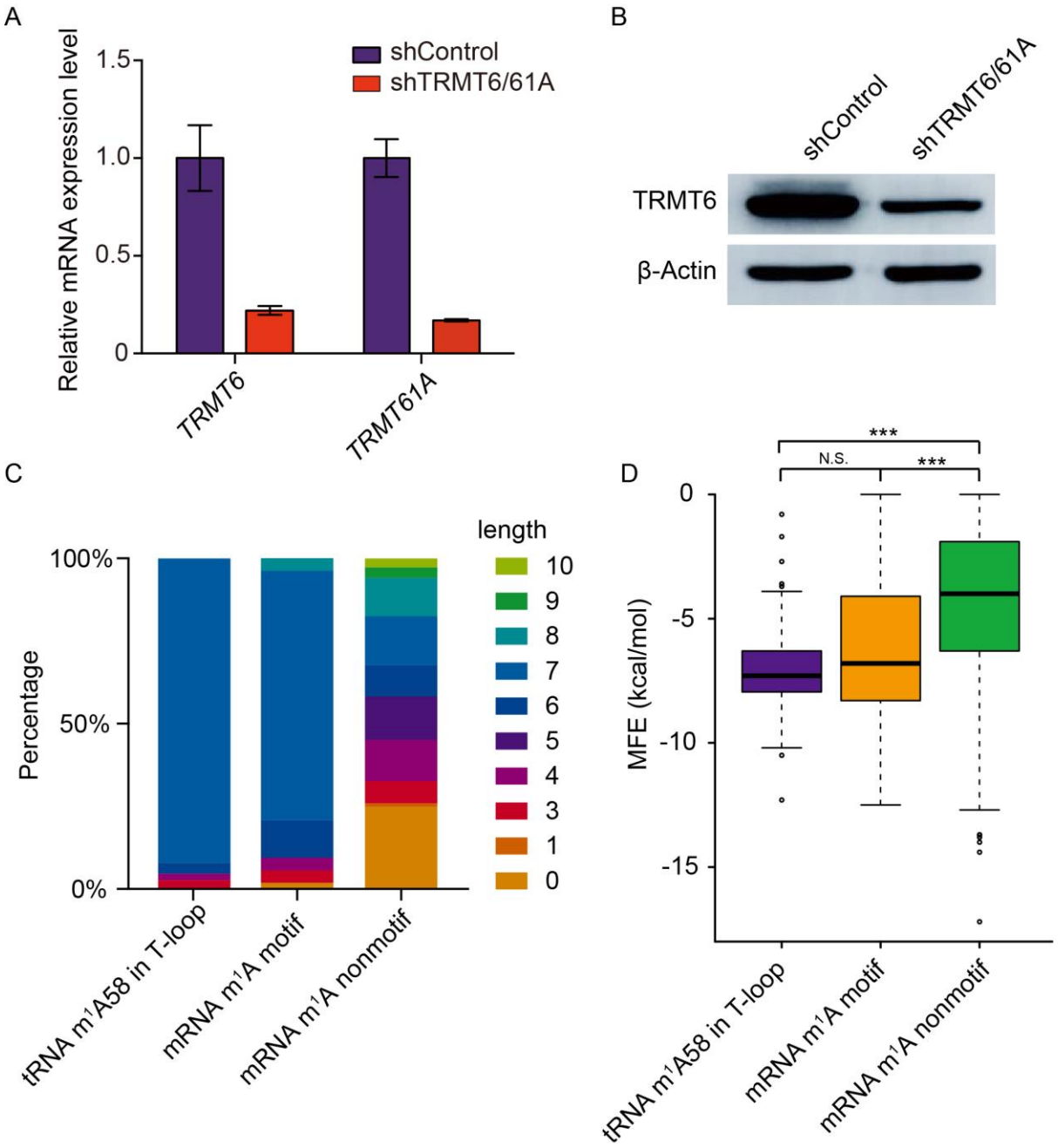

Figure S4. The tRNA methyltransferase complex TRMT6/61A catalyzes a subset of m^{1}A methylation in mRNA, Related to Figure 3.

(**A**) The mRNA level of TRMT6 and TRMT61A in the TRMT6/61A knock-down cells was quantified by qPCR. Data are represented as mean ± SD; n = 4.

(**B**) The protein expression level of TRMT6 in the TRMT6/61A knock-down cells was determined by Western blot. β-Actin was used as a loading control.

(**C**) The length of m^1A-containing loops was calculated for m^1A in tRNA and mRNA. The GUUCRA mRNA m^1A sites are confined to a hairpin structure most frequently with a 7nt loop, resembling the feature of m^1A58 in tRNA. Such observation is not observed for the non-motif mRNA m^1A sites.

(**D**) Minimum free energy (MFE) was calculated for the predicted local structure of m^1A-containing sequence in tRNA and mRNA (see Method Details). The mRNA m^1A site within the GUUCRA motif tends to reside in a more stable structure, which is similar to the context of m^1A58 in tRNA; while the non-motif mRNA m^1A sites are generally located within less stable structures.

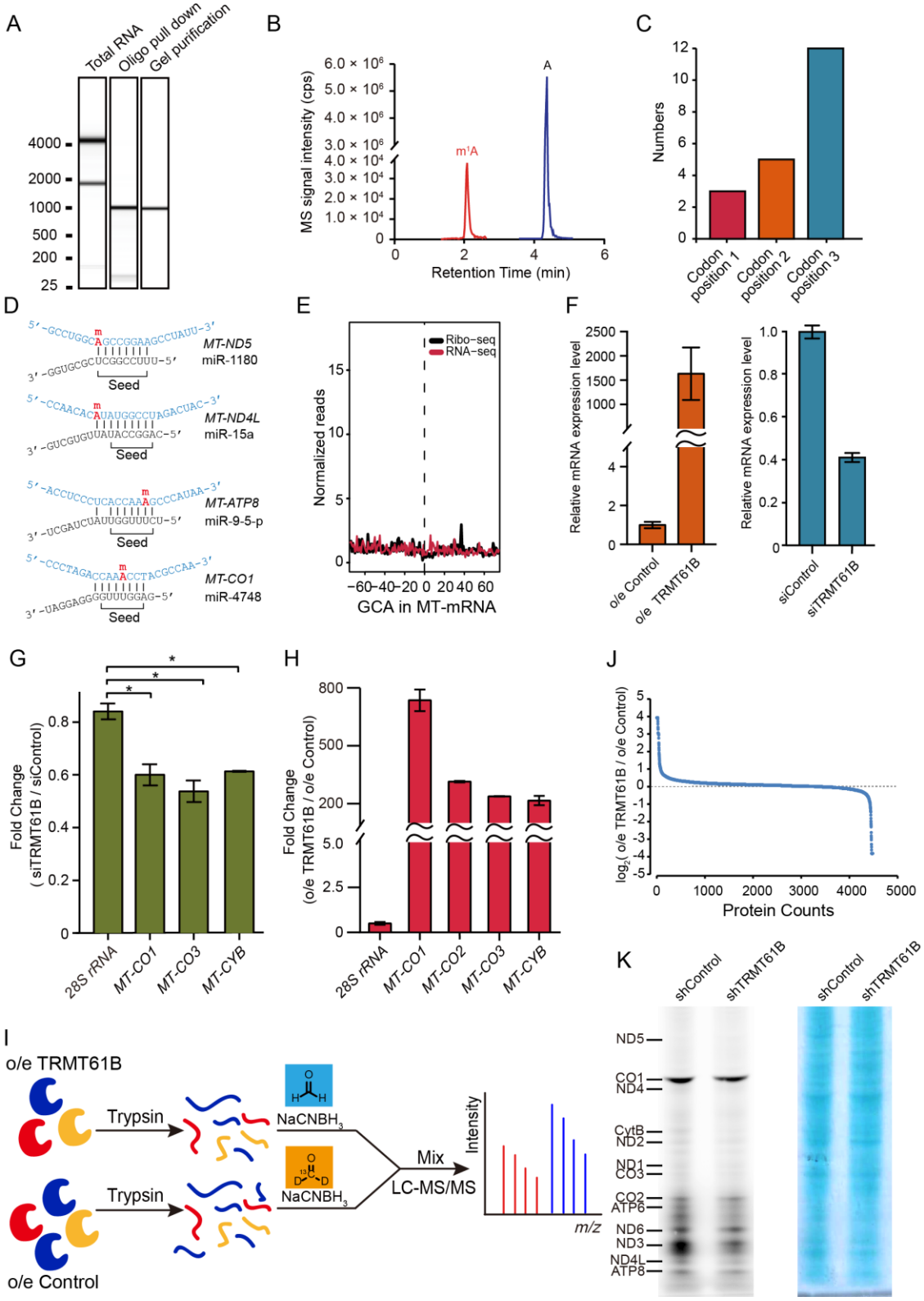

Figure S5. The mitochondrial m^{1}A methylome and its role in the regulation of mitochondrial translation, Related to Figure 4 and 5.

(**A**) The purity of the isolated 12S mt-rRNA was analyzed by the Bioanalyzer 2100 instrument.

12S mt-rRNA was first isolated using several specific antisense oligonucleotides (as “oligo pull down”) and further purified by an additional Urea-PAGE gel purification step (as “gel purification”).

(**B**) The m^1A modification level of 12S mt-rRNA was measured by quantitative mass spectrometry (LC-MS/MS), showing that its m^1A/A ratio is ~0.1%.

(**C**) The numbers of m^1A sites in different codon positions are shown. m^1A appears to be preferentially present at the third position of a codon in the CDS of mt-mRNA.

(**D**) The m^1A sites in *MT-ND5* and *MT-ND4L* reside exactly within mRNA sequences that form base-pairing with the seed regions of microRNAs, as shown by the published miRNA CLASH results. Two additional m^1A sites in *MT-ATP8 and MT-CO1* were found to be within the predicted mt-mRNA targets of the microRNA seed regions.

(**E**) m^1A1374 in *MT-ND5* is located in an Ala(GCA) codon and causes ribosome stalling. As a control, the normalized density of the 5’ end of footprints was calculated for positions surrounding all GCA codons in mt-mRNA, showing no pausing signal at GCA codons in general.

(**F**) The relative mRNA levels in the TRMT6/61B over-expression and knock-down cells are shown, respectively. Data are represented as mean ± SD; n = 4.

(**G**) The modification levels of three mt-mRNA transcripts in TRMT6/61B knock-down cells were quantified using the qPCR-based assay. m^1A level shows a mild yet significant decrease in the TRMT61B knock-down cells. The significance test was performed with two-tailed Student’s t test for paired samples. Data are represented as mean ± SD; n = 2.

(**H**) The modification levels of four mt-mRNA transcripts in TRMT6/61B overexpression cells were quantified using the qPCR-based assay. m^1A level shows a dramatic increase in the TRMT61B overexpression cells. Data are represented as mean ± SD; n = 2.

(**I**) Experimental procedure for quantitatively measuring the protein level upon TRMT61B over-expression.

(**J**) The global expression level of the proteome of the whole cells was not changed upon TRMT61B over-expression.

(**K**) Detection of nascent mitochondrial protein synthesis in the mock control and TRMT61B knock-down cell lines. After knock-down for 96h, the cytoplasmic translation was inhibited by the addition of emetine while nascent mitochondrial proteins were labeled with AHA. As shown in the figure, the nascent protein level of non-targets (MT-ATP6, MT-ATP8, MT-ND3 and MT-ND4L) significantly decreased upon TRMT61B knock-down, presumably due to the decreased modification level of TRMT61B-dependent m^1A sites in mt-rRNA and mt-tRNA. Coomassie blue staining was used as the loading control.